Computations of neoclassical transport in stellarators using a δf method with reduced variance *

Klaus ALLMAIER[1)], Sergei V. KASILOV[1,2)], Winfried KERNBICHLER[1)], Georg O. LEITOLD[1)], Viktor V. NEMOV[1,2)]

[1)] *Association EURATOM-ÖAW, Institut für Theoretische Physik - Computational Physics, TU Graz, Petersgasse 16, A–8010 Graz, Austria*

[2)] *Institute of Plasma Physics, National Science Center "Kharkov Institute of Physics and Technology", Akademicheskaya Str. 1, 61108 Kharkov, Ukraine*

An improved δf Monte Carlo method for the computation of neoclassical transport coefficients in stellarators is presented. Compared to the standard δf method without filtering, the computing time needed for the same statistical error decreases by a factor proportional to the mean free path to the power 3/2.

Keywords: bootstrap current, stellarator, δf Monte Carlo, variance reduction

A standard δf Monte Carlo method for the computation of neoclassical transport coefficients [1] assumes solution of the linearized drift-kinetic equation taking into account the source term in the equation for test particle weights which evolve with time. This method has a good convergence for tokamaks where the variance in all transport coefficients including bootstrap coefficient has no strong dependence on plasma collisionality. However, in stellarators, the variance in the bootstrap coefficient increases for this method as a square of the mean free path due to the accumulation of large random contributions to the test particle weights which occur in the phase space region occupied by trapped particles. In Ref. [2] a method has been presented which is a combination of the standard Monte Carlo method with a method employing constant particle weights and re-discretizations of the test particle distribution in phase space. There, this method has been tested in confinement regimes with negligible radial electric field. Below this method is described in more detail for general confinement regimes.

Mono-energetic transport coefficients are determined by the steady state solution of the linearized drift kinetic equation for the normalized perturbation of the distribution function $\hat{f}$ (marker)

$$\mathcal{L}_D \hat{f} \equiv \left(\frac{\partial}{\partial t} + \mathbf{V}_g \cdot \nabla - \mathcal{L}_C \right) \hat{f} = \dot{\psi} \equiv \mathbf{V}_g \cdot \nabla \psi, \qquad (1)$$

where $\mathcal{L}_C$, $\mathbf{V}_g$, and $\dot{\psi}$ are Lorentz collision operator, drift velocity and its co-variant ψ-component, respectively, and velocity space variables are total energy and perpendicular adiabatic invariant. Here, ψ is a flux surface label, and a marker is defined through the local Maxwellian distribution function f_M and the total distribution function f via $f = f_M - \hat{f} \partial f_M / \partial \psi$. The mono-energetic radial diffusion coefficient and the normalized bootstrap coefficient, respectively, are given by

$$D_{\mathrm{mono}} = -\frac{1}{\langle |\nabla \psi| \rangle^2} \left\langle \frac{1}{2} \int_{-1}^{1} \mathrm{d}\lambda \hat{f} \dot{\psi} \right\rangle, \qquad (2)$$

$$\lambda_{bb} = -\frac{3}{\rho_L B_0 \langle |\nabla \psi| \rangle} \left\langle \frac{1}{2} \int_{-1}^{1} \mathrm{d}\lambda \hat{f} \lambda B \right\rangle, \qquad (3)$$

where $\lambda = v_\parallel / v$ is the pitch parameter, ρ_L is the Larmor radius in the reference magnetic field B_0, B is the magnetic field module and $\langle \ldots \rangle$ denotes the average over the volume between neighboring flux surfaces. The quantity λ_{bb} is linked to the equilibrium (bootstrap) current density $j_\parallel$ and gradient of the pressure p by $\lambda_{bb} = -\langle j_\parallel B \rangle (c \langle |\nabla \psi| \rangle \mathrm{d}p/\mathrm{d}\psi)^{-1}$. In the following D_{mono} is normalized by the plateau diffusion coefficient $D_{\mathrm{plateau}} = \pi v \rho_L^2 (8\sqrt{2} \iota R)^{-1}$ where ι and R are the rotational transform and major radius, respectively.

In order to introduce the Monte Carlo operator it is convenient to re-write (1) in the integral form using a Green's function G defined by

$$\mathcal{L}_D \, G(t, \mathbf{z}, \mathbf{z}_0) = 0 \qquad (4)$$

$$G(0, \mathbf{z}, \mathbf{z}_0) = (g(\mathbf{z}_0))^{-1/2} \, \delta(\mathbf{z} - \mathbf{z}_0), \qquad (5)$$

where $\mathbf{z} = (\vartheta, \varphi, \lambda)$ and g is a metric determinant of flux coordinates $(\psi, \vartheta, \varphi)$. This Green's function is normalized to 1,

$$\int \mathrm{d}^3 z \, (g(\mathbf{z}))^{1/2} \, G(t, \mathbf{z}, \mathbf{z}_0) = 1. \qquad (6)$$

*This work, supported by the European Communities under the contract of Association between EURATOM and the Austrian Academy of Sciences, was carried out within the framework of the European Fusion Development Agreement. The views and opinions expressed herein do not necessarily reflect those of the European Commission. Additional funding is provided by the Austrian Science Foundation, FWF, under contract number P16797-N08.

author's e-mail: allmaier@itp.tugraz.at

Thus, a formal solution to Eq. (1) is

$$\hat{f}(t,\mathbf{z}) = \int \mathrm{d}^3 z_0 \,(g(\mathbf{z}_0))^{1/2} \Bigg(G(t-t_0,\mathbf{z},\mathbf{z}_0)\hat{f}(t_0,\mathbf{z_0}) \times \int_{t_0}^{t} \mathrm{d}t' G(t-t',\mathbf{z},\mathbf{z}_0)\dot{\psi}(\mathbf{z_0}) \quad (7)$$

If a steady state solution is looked for, $\hat{f}(t,\mathbf{z}) = \hat{f}(\mathbf{z})$, Eq. (7) becomes an integral equation for $F(\mathbf{z}) = (g(\mathbf{z}))^{1/2}\,\hat{f}(\mathbf{z})$ given below also in the operator form,

$$F(\mathbf{z}) = \int \mathrm{d}^3 z_0 K(\mathbf{z},\mathbf{z}_0)F(\mathbf{z_0}) + Q(\mathbf{z}) \equiv \mathcal{K}F + Q, \quad (8)$$

where $K(\mathbf{z},\mathbf{z}_0) = (g(\mathbf{z}))^{1/2}\,G(\Delta t,\mathbf{z},\mathbf{z}_0)$, Δt is the integration time step and

$$Q(\mathbf{z}) = \int \mathrm{d}^3 z_0 \,(g(\mathbf{z})g(\mathbf{z}_0))^{1/2} \int_0^{\Delta t} \mathrm{d}t' G(t',\mathbf{z},\mathbf{z}_0)\dot{\psi}(\mathbf{z_0}) \approx (g(\mathbf{z}))^{1/2}\,\dot{\psi}(\mathbf{z})\Delta t. \quad (9)$$

Introducing the Monte Carlo operator, $\mathbf{Z}(\Delta t,\mathbf{z}_0)$, being the random position of a test particle starting at $\mathbf{z}_0$ after a single time step modeled in a standard way [4] by the random change of λ in accordance with $\mathcal{L}_C$ and integration of particle drift equations, the kernel of the integral equation is given by an expectation value $K(\mathbf{z},\mathbf{z}_0) = \overline{\delta\,(\mathbf{z}-\mathbf{Z}(\Delta t,\mathbf{z}_0))}$.

The solution of (8) by direct iterations can be presented as an expectation value of an integral along the stochastic orbit,

$$F = \sum_{k=0}^{\infty}\mathcal{K}^k Q = C_0 \sum_{k=0}^{\infty} \overline{w_0\,\delta\,(\mathbf{z}-\mathbf{z}_k)}, \quad (10)$$
$$\mathbf{z}_k = \mathbf{Z}(\Delta t,\mathbf{z}_{k-1}), \qquad w_0 = \dot{\psi}(\mathbf{z}_0)\Delta t,$$

where $C_0 = \int \mathrm{d}^3 z\,(g(\mathbf{z}))^{1/2}$ and the random starting point $\mathbf{z}_0$ is chosen with the probability density $\overline{\delta\,(\mathbf{z}-\mathbf{z}_0)} = C_0^{-1}\,(g(\mathbf{z}))^{1/2}$. The averages (2) and (3) are given by expectation values as

$$D_{\mathrm{mono}} = -\frac{1}{\langle|\nabla\psi|\rangle^2}\sum_{k=0}^{\infty}\overline{w_0\dot{\psi}(\mathbf{z}_k)}, \quad (11)$$

$$\lambda_{bb} = -\frac{3}{\rho_L B_0\,\langle|\nabla\psi|\rangle}\sum_{k=0}^{\infty}\overline{w_0\lambda_k B(\mathbf{z}_k)}. \quad (12)$$

When $k\Delta t$ exceeds a few collision times, the correlation between $\mathbf{z}_k$ and w_0 is lost and, therefore, such terms in (11) tend to zero, e.g. $\overline{w_0\dot{\psi}(\mathbf{z}_k)} \to \overline{w_0}\;\overline{\dot{\psi}(\mathbf{z}_k)} = 0$ because the expectation value $\overline{w_0} = C_0^{-1}\Delta t\int \mathrm{d}^3 z\,(g(\mathbf{z}))^{1/2}\,\dot{\psi}(\mathbf{z}) = 0$ due to Liouville's theorem. Thus, a finite sum over k is sufficient in (11). The method of constant test particle weights described by (11) and (12) has rather low variance in computations of D_{mono}, however, for λ_{bb} variance has a very unfavorable scaling with collisionality. Indeed, only the orbits originating in the boundary layer in velocity space of the width $\Delta\lambda \sim (L_c/l_c)^{1/2}$ where $L_c = 2\pi R/\iota$ and $l_c = v\tau_c$ are the connection length and mean free path, respectively, contribute to λ_{bb}. In addition, the contribution of a particle from the boundary layer is $\Delta\lambda$ times smaller than of a normal passing particle because of a higher trapping probability. Therefore, the variance in λ_{bb} scales for this method as $(l_c/L_c)^2$ in the long mean free path regime.

It should be noted that distribution of test particles after each step remains to be the equilibrium distribution, $\overline{\delta\,(\mathbf{z}-\mathbf{z}_k)} = C_0^{-1}\,(g(\mathbf{z}))^{1/2}$.

Therefore $\overline{w_0\lambda_{k-j}B(\mathbf{z}_{k-j})} = \overline{w_j\lambda_k B(\mathbf{z}_k)}$ where $w_j = \dot{\psi}(\mathbf{z}_j)\Delta t$, and

$$\sum_{k=0}^{\infty}\overline{w_0\lambda_k B(\mathbf{z}_k)} = \lim_{k\to\infty}\overline{W_k\lambda_k B(\mathbf{z}_k)} \quad (13)$$

$$= \lim_{K\to\infty}\frac{1}{K}\sum_{k=0}^{K}\overline{W_k\lambda_k B(\mathbf{z}_k)}, \quad (14)$$

$$W_k = \sum_{j=0}^{k} w_j. \quad (15)$$

The procedure in (13) corresponds to a standard δf method [1] where the test particle weight W_k is an integral of $\dot{\psi}$ along a stochastic orbit. In a tokamak, the variance in λ_{bb} does not scale with the collisionality, and the required CPU time for this method scales linearly with l_c/L_c. However, in stellarators variance in λ_{bb} again recovers the scaling $(l_c/L_c)^2$ because due to the non-zero bounce-averaged drift of trapped particles large contributions to W_k are acquired, which scale as $\dot{\psi}\tau_c$ and which become weakly correlated with the values of λ_k after detrapping of test particles. To overcome this problem, in Ref. [5] trapped particles with large W_k are replaced with particles with $W_k = 0$ (large weights are filtered out) which formally introduces some bias in the result.

For a formally "unbiased" method it is convenient to split the source in (8) into "passing" and "trapped" sources $Q_p = \chi Q$ and $Q_t = Q - Q_p$ using

$$\chi = \frac{1}{2}\Big(1 + \tanh\Big((\lambda-\lambda_{t-p})/\Delta\lambda\Big)\Big), \quad (16)$$

where λ_{t-p} is a trapped-passing boundary, and solve the problem with each source independently. Results for transport coefficients for these two sources are added up at the end. The problem with Q_p is solved with the standard method (13) because accumulation of large weights is avoided there. For the problem with Q_t the formal solution to (8) is presented as $F = F_M + \Delta F_M$ where F_M satisfies an equation which differs from (8) only by a source term,

$$F_M = \mathcal{K}F_M + Q_M, \quad (17)$$

where

$$Q_M = \frac{1}{M}\sum_{k=0}^{M-1}\mathcal{K}^k Q, \quad (18)$$

$$\Delta F_M = \sum_{k=0}^{M-1}\left(1-\frac{k+1}{M}\right)\mathcal{K}^k Q. \quad (19)$$

In order to derive (17) the original equation (8) is presented as

$$F = \sum_{k=0}^{m-1} \mathcal{K}^k Q + \mathcal{K}^m F, \qquad (20)$$

where m is an arbitrary natural number. Averaging the r.h.s. of (20) over $1 \le m \le M$ yields

$$F = \Delta F_M + \frac{1}{M}\left(\sum_{m=0}^{M-1} \mathcal{K}^m Q + \sum_{m=1}^{M} \mathcal{K}^m F\right) \qquad (21)$$

Denoting the last term in (21) with F_M and substituting there F in the form of the series (10) one obtains

$$F_M \equiv \frac{1}{M}\left(\sum_{m=0}^{M-1} \mathcal{K}^m Q + \sum_{m=1}^{M} \mathcal{K}^m F\right) \qquad (22)$$

$$= \sum_{k=0}^{\infty} \mathcal{K}^k Q_M, \qquad (23)$$

which is a series solution to Eq. (17).

Equation (17) describes one iteration of the solution procedure. Given the source term Q such iteration provides Q_M which is used as a source term Q for the next iteration. Within an iteration, each of the test particles performs $M-1$ steps, and the quantity Q_M is computed by scoring weights on the 3D grid (except the first iteration). The contribution of the iteration to the distribution function, ΔF_M, is formally used in the averages (2) and (3) so that they are computed directly in analogy to (11) and (12). For the first iteration with Q being the original source (9) the algorithm with alternating weights (15) is used. After the first iteration these test particle weights are divided by M so that test particles represent the discretized distribution Q_M used as a source within the second iteration. Starting from this second iteration, an algorithm with fixed test particle weights (and scoring Q_M on the grid) is used. After the second iteration, the module of test particle weight is fixed. Due to annihilation of the weights on the grid and fixed module of the weight, the number of test particles needed for sampling the source term from the grid is decreasing with iterations and iterations are stopped when this number is below one, (see Fig. 1). The number of steps M for a single iteration is chosen to be much smaller than collision time and large enough in order to fill the grid using a limited number of test particles. Since source terms generated in this way are small in the passing and boundary region, particles are generated there with smaller weights and particles which enter the boundary layer from the trapped side are split in such a way that the number of test particles in the passing and trapped regions is of the same order. As a result, variance of this method is reduced to the scaling l_c/L_c. In addition, due to the decay of test particle number with iterations, the CPU time is also reduced and scales as $(l_c/L_c)^{3/2}$ for a given accuracy (see Fig. 2) which is much better than the scaling $(l_c/L_c)^3$ of the standard δf method without a filter. Results of testing of the method for a few toroidal devices stay in good agreement with results of NEO-2, a field

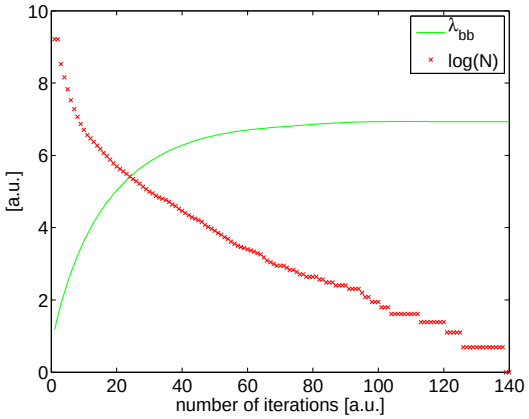

Fig. 1 Bootstrap coefficient λ_{bb} (green) and logarithm of the number of simulation particles (red) plotted over the number of iterations.

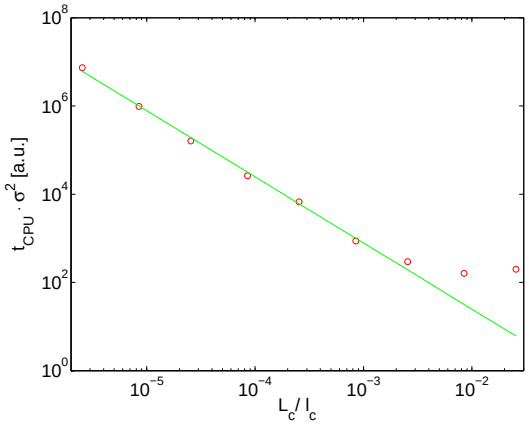

Fig. 2 CPU-time multiplied with the variance of the bootstrap coefficient σ^2 plotted over the collisionality parameter (red). The green line shows the scaling $(l_c/L_c)^{3/2}$.

line tracing code which computes transport coefficients in arbitrary collisionality regimes [3], as shown in Figs. 3-6. Benchmarking of the results from computations with finite radial electric fields with other methods has been started, first results can be found in Ref. [6].

[1] M. Sasinowski and A.H. Boozer, Phys. Plasmas **2**, 610 (1995).

[2] K. Allmaier, S. V. Kasilov, W. Kernbichler, G. O. Leitold and V. V. Nemov, *34th EPS Conference on Plasma Physics, Warsaw, 02–06 July 2007*, P-4.041, (2007).

[3] W. Kernbichler, S. V. Kasilov, G. O. Leitold, V. V. Nemov, and K. Allmaier, *33rd EPS Conference on Plasma Physics, Rome, 19–23 June 2006*, ECA Vol. **30I** P-2.189, (2006).

[4] A. H. Boozer and G. Kuo-Petravic, Phys. Fluids **24**, 851 (1981).

[5] M. Yu. Isaev, S. Brunner, W. A. Cooper, et al., Fusion Science & Technology **50**, 440 (2006).

[6] K. Allmaier, C.D. Beidler, M.Yu. Isaev, S.V. Kasilov, W. Kernbichler, H. Maassberg, S. Murakami, D.A. Spong, V. Tribaldos, *ICNTS - Benchmarking of Bootstrap Current Coefficients*, this workshop, (2007).

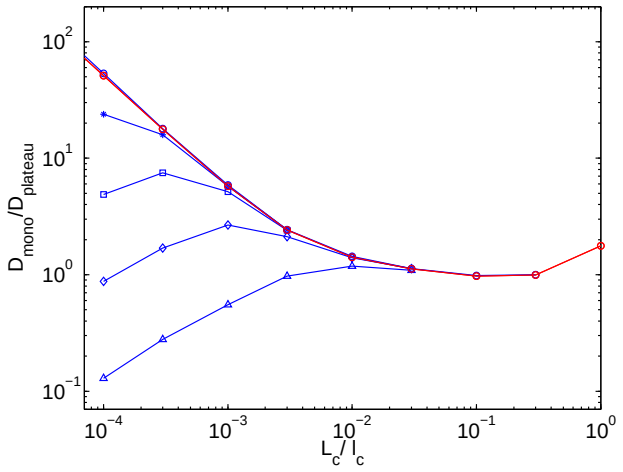

Fig. 3 Normalized diffusion coefficient $D_{\mathrm{mono}}/D_{\mathrm{plateau}}$ for LHD with R=375cm vs. collisionality parameter L_c/l_c at half plasma radius computed by NEO-MC (blue) and NEO-2 (red) for $E_r/v/B = 0$ (circles), $3 \cdot 10^{-5}$ (stars), $1 \cdot 10^{-4}$ (squares), $3 \cdot 10^{-4}$ (diamonds), $1 \cdot 10^{-3}$ (triangles)

.

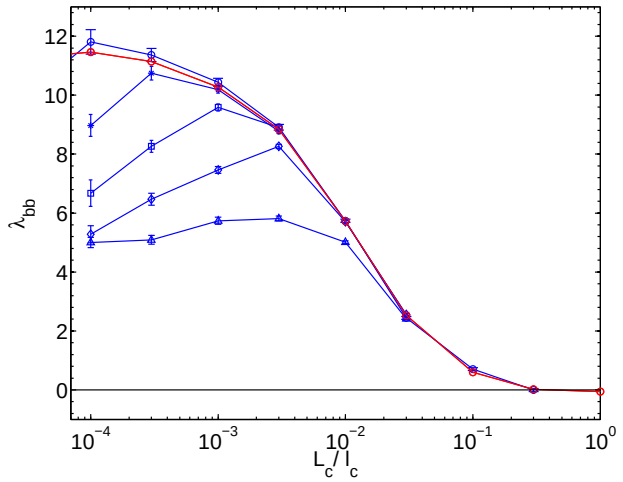

Fig. 4 Normalized bootstrap coefficient λ_{bb} for LHD with R=375cm vs. collisionality parameter L_c/l_c at half plasma radius. Markers and colors are the same as in Fig. 3

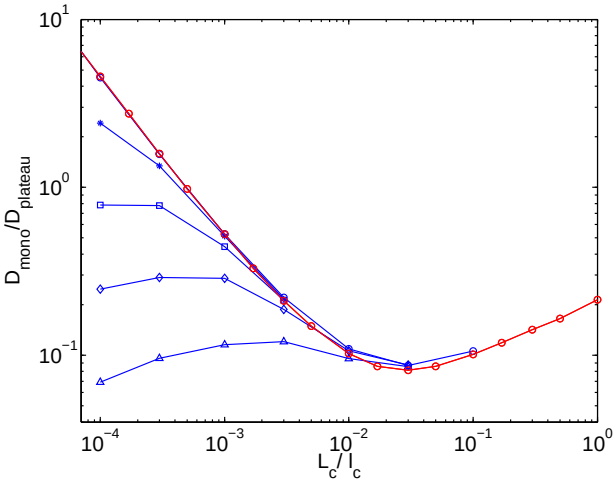

Fig. 5 Normalized diffusion coefficient $D_{\mathrm{mono}}/D_{\mathrm{plateau}}$ for W7-X standard configuration vs. collisionality parameter L_c/l_c at half plasma radius. Markers and colors are the same as in Fig. 3

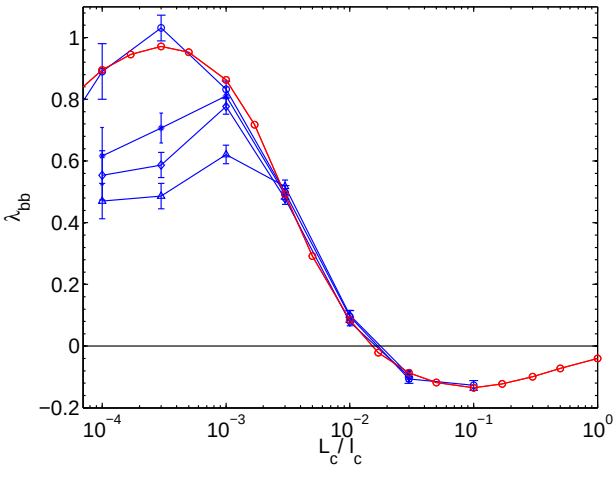

Fig. 6 Normalized bootstrap coefficient λ_{bb} for W7-X standard configuration vs. collisionality parameter L_c/l_c at half plasma radius. Markers and colors are the same as in Fig. 3